# CHAPTER 3

## SIMULATION INVESTIGATIONS OF UNIFORM DIELECTRIC LOADED FUNDAMENTAL HARMONIC GYRO-TWT*



*Part of this work has been published as:

**Akash** and M. Thottappan, "Stability and Multimode Simulation Studies of W-Band Uniformly Dielectric-Loaded Gyrotron Traveling-Wave Tube Amplifier," *IEEE Trans. Electron Devices,* vol. 66, no. 12, pp. 5305-5312, Dec. 2019 (10.1109/TED.2019.2944487).

## 3.1. Introduction

In this chapter, the PIC simulation study of a W-band gyro-TWT amplifier is presented. To suppress the parasitic modes, the interaction structure of gyro-TWT has been loaded with a uniformly distributed lossy dielectric layer. The effect of lossy dielectric layer on the propagation of operating and parasitic modes has been studied. The lossy dielectric layer provides heavy attenuation to the parasitic backward wave oscillating modes so that their strength become too weak to oscillate at the operating beam current. The lossy layer also weakens the strength of operating mode as well but sufficient to grow exponentially in the nonlinear (unloaded) section. The resistivity of the lossy layer is kept 70,000 times copper's resistivity. At this resistivity, a total of 90dB / 12 cm insertion loss to operating mode $TE_{01}$ has been predicted by the cold simulation. The PIC simulation results are validated with the multimode code based on the multimode theory discussed in Chapter 2. Further, the design and simulation studies of various subassemblies of gyro-TWT amplifier for the present W-band $TE_{01}$ mode gyro-TWT have been presented. A single anode MIG is used here to emit the gyrating electron beam of 100kV and 5A with 5% axial velocity spread. A novel $TE_{01}$ mode input coupler with Y-shaped power divider circuit is presented to feed the desired operating mode to the gyro-TWT. Further, to extract the RF power a single disk microwave window and collect the spent beam an unrepressed collector are also studied.

## 3.2. Design of Input System of $TE_{01}$ mode W-band Gyro-TWT

The magnetron injection gun (MIG) and input coupler are the main components of the input system of a gyro-TWT amplifier. In this chapter, a single anode (diode) MIG is designed and simulation using EGUN code. Also, a novel $TE_{01}$ mode input coupler with Y-shaped power divider circuit is designed and simulated to feed the gyro-

TWT with the operating $TE_{01}$ mode. A detailed study of both MIG and input coupler is discussed independently in the following sections.

### 3.2.1. Single Anode Magnetron Injection Gun

A single anode MIG for 92 GHz gyro-TWT is designed using E-GUN code [Herrmann Feldt (1988)]. The design parameters and simulation results are listed in Table 3.1. MIG basically consists of three regions including cathode region, anode region and magnetic field compression region [Baird *et al.* (1986)]. The main goal of the design of MIG for gyro-TWT is to obtain the minimum axial velocity spread and an optimum velocity ratio. 2D geometry of present electron gun (Figure 3.1) shows the beam trajectory, B-field profile, and equipotential lines. For the present design, the required DC beam values are 100kV beam voltage and 5A beam current. The parametric analysis of emitted electron beam is done by varying the anode voltage and beam current [Figure 3.2(a) and 3.2(b)]. The electron gun has been found to have velocity ratio of 1.01 and minimum axial velocity spread of 5 % at an anode voltage of 100kV and 5A current.

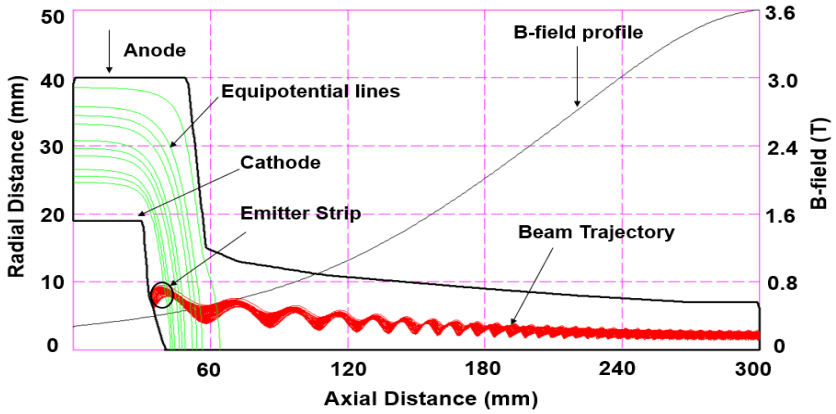


**Figure 3.1:** Electron beam trajectory, B-field profile and equipotential lines for W-band Magnetron injection Gun simulated using EGUN code.

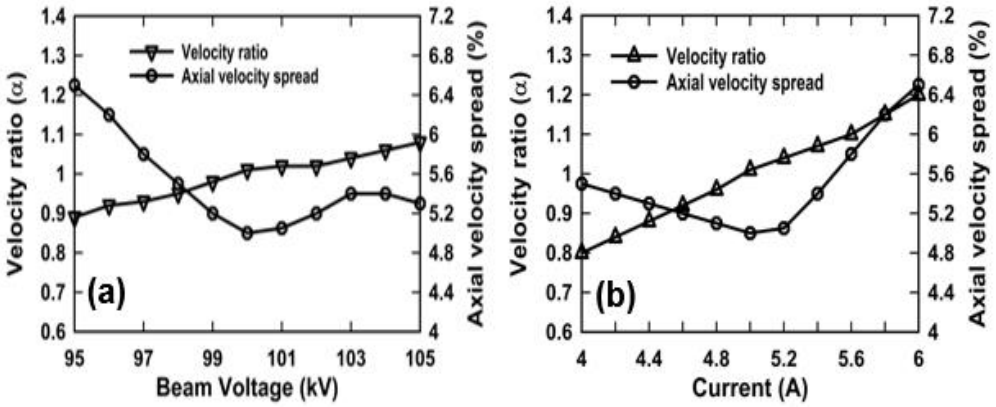


**Figure 3.2:** Velocity ratio and axial velocity spread for different value of (a) anode voltage and (b) beam current.

### 3.2.2. Y-shape $TE_{01}$ mode Input Coupler

The main role of an input coupler is to feed the RF input signal into the cavity or waveguide. The feeding at higher order mode operation always requires a mode convertor that converts the fundamental mode into a desired operating mode. As per the requirement of gyro-TWT, the input coupler should have high mode purity, good transmission and low reflections with broad bandwidth without any mode competition. In order to fulfill these requirements, a Y-shaped input coupler [Yu *et al.* (2005)] is designed which includes a cascaded Y-shaped power divider circuit and a side wall coupling based quad fed mode-converter. The cascaded Y-shaped geometry splits the rectangular $TE_{10}$ mode input signal into four signals with equal amplitude and a phase difference $90^0$. These four signals are further given as the input to quad fed mode convertor. The quad fed mode convertor converts the rectangular $TE_{10}$ mode into circular $TE_{01}$ mode through the side wall coupling. The present input coupler is modeled and simulated using "CST Microwave Studio". The design parameters of the input coupler are listed in Table 3.2. The E-field contour plot of input $TE_{10}$ mode in rectangular waveguide and desired circular $TE_{01}$ mode in cylindrical waveguide is shown in Figure 3.3(a). The cold simulation behavior of the present input coupler

[Figure 3.3(b)] shows that the transmission loss ($S_{21}$) is ~0.05 dB and the reflection ($S_{11}$) is more than -20 dB at the desired operating frequency. The present input coupler having high mode purity with low reflection and the transmission coefficient ($S_{21}$) of other modes is less than -50dB at the operating frequency.

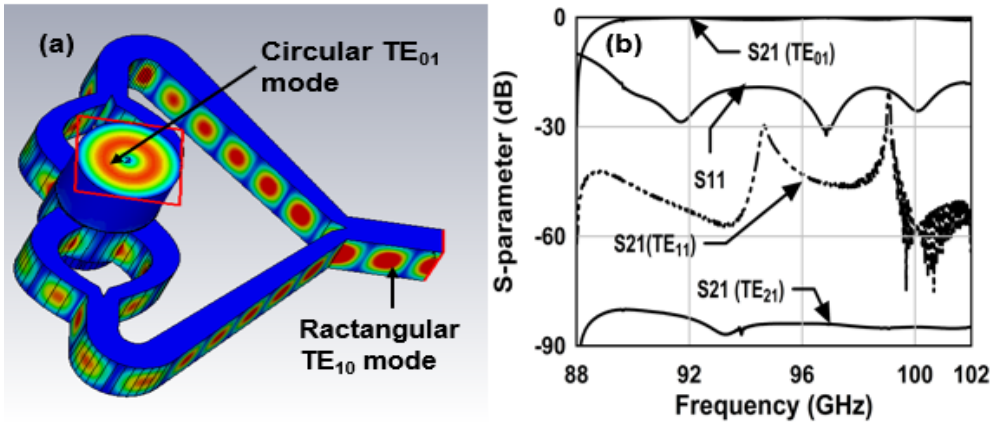


**Figure 3.3:** (a) CST model of Y-shape input coupler along with E-field contour plot (b) S-parameter results for input coupler.

**Table 3.1**: Design parameters for diode MIG

| Parameters | Dimension |
|---|---|
| Anode potential, $V_a$ | 100 kV |
| Slant angle of Emitter, $\varphi_c$ | $29^0$ |
| Length of Emitter Strip, $L$ | 2 mm |
| Axial Velocity spread | 5 % |
| Velocity ratio (α) | 1.01 |
| Compression ratio, $f_m$ | 30 |
| Current density, $J_c$ | 8.8 A/cm$^2$ |

**Table 3.2**: Design Parameters for Input Coupler

| Parameters | Dimension |
|---|---|
| Rectangular Waveguide (WR-10) | 2.87*1.435 mm |
| Cylindrical waveguide radius ($r_w$) | 2.01 mm |
| Cylindrical waveguide length | 4.0 mm |
| Drift Tube radius ($r_d$) | 0.8*$r_w$ |
| Drift Tube length | 3.0 mm |

## 3.3. Design of Beam-wave Interaction Structure

### 3.3.1. Dispersion and Beam-wave Coupling Impedance

The dispersion [Figure 3.4(a)] of the present gyro-TWT shows that the intersection between the fundamental cyclotron harmonic (s = 1) beam mode line and waveguide $TE_{01}$ mode curve in the positive $k_z$ region causes the convective instability for the amplification of RF wave. Similarly, intersections of $TE_{11}$ and $TE_{21}$ modes with fundamental (s = 1) and intersection of $TE_{02}$ mode with second (s = 2) harmonic beam mode lines in the negative $k_z$ region causes the absolute instability in the amplifier.

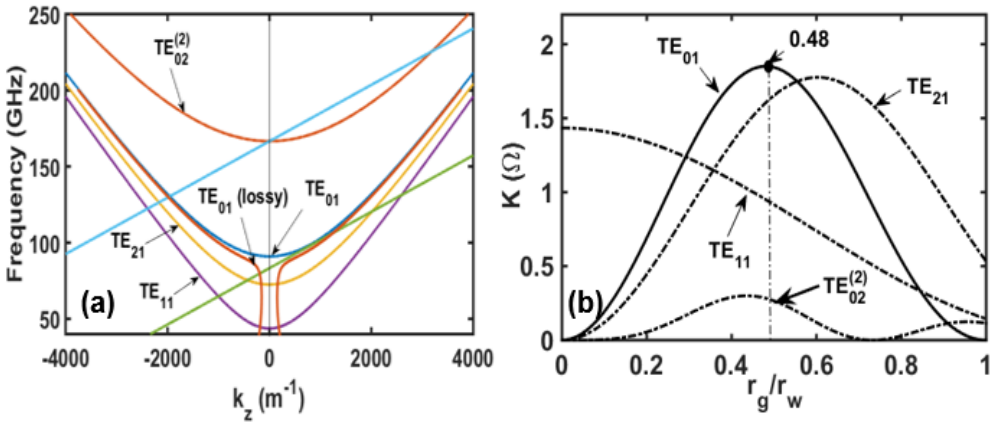


**Figure 3.4:** (a) Dispersion of UDL gyro-TWT operating at 92 GHz for 100 kV, 5 A, and (b) coupling impedance Vs normalized guiding center radius for operating and competing modes.

The oscillation frequencies of these competing modes including $TE_{11}$, $TE_{21}$, and $TE_{02}$ (s = 2) are observed as ~67 GHz, ~77 GHz, and ~166.5 GHz, respectively. For the lossy waveguide, the dispersion curve of $TE_{01}$ mode is discontinuous near the cut-off region, because the solution of dispersion, $D(\omega, k_z) = 0$, which results in a complex $k_z$ value and its imaginary part is much larger than the real $k_z$. Thus, it leads to higher attenuation to the modes, which are nearer to the cut-off. The coupling impedance [Du *et al.* (2010)] is maximum for the operating $TE_{01}$ mode at a beam radius of $0.48r_w$ [Figure 3.4(b)]. Though, the coupling strength of $TE_{01}$ mode at this point is higher than the coupling

strength of $TE_{11}$ and $TE_{02}$ modes, but it is comparable to $TE_{21}$ mode. To minimize the interception of electrons with wall and to reduce the coupling of the desired operating mode with spurious modes ($TE_{11}$, $TE_{21}$, and $TE_{02}$), the beam radius is chosen as 0.45 $r_w$.

### 3.3.2. Backward-Wave Oscillations and Stability Analysis

The present gyro-TWT consists of a linear region, which is loaded with aquadag graphite material having the resistivity between 36000 $\rho_{Cu}$ - 80,000 $\rho_{Cu}$ [Chu *et al.* (1999)]. This lossy section is meant for suppressing the potential BWOs by attenuating them. The axial wave propagation constant for a lossy waveguide after considering the effect of lossy layer thickness ( $\Delta r$ ) can be given as [Du *et al.* (2008)],

$$k_z = \left[ \frac{\omega^2}{c^2} - \left( \frac{x_{mn}}{r_w} \right) \times \left\{ \begin{array}{l} 1-(1-\mathrm{i})\dfrac{\delta}{r_w}\tan\left( \Delta r \times \dfrac{1+i}{\delta} \right) \\ \left( 1+\dfrac{m^2}{x_{mn}^2 - m^2}\dfrac{\omega^2}{\omega_n^2} \right) \end{array} \right\} \right]^{1/2} \tag{3.1}$$

where, $\delta$ is the skin depth, $\omega_n$ is the cut-off angular frequency and the term $\tan((1+i)\Delta r / \delta)$ is called as thickness factor. The variation of thickness factor with respect to relative thickness ($\Delta r/\delta$) of the lossy layer [Figure 3.5(a)], shows that the propagation constant is sensitive to the value of relative thickness below 1.5 and is saturated beyond that. Also, the attenuation to $TE_{01}$ mode increases as the resistivity of the lossy material increases [Figure 3.5(b)]. The attenuation and phase constants of the operating $TE_{01}$ mode as a function of frequency for different value of thickness are shown in Figure 3.6(a) and 3.6(b), respectively. It can be seen from the figure that the attenuation to the operating mode decreases and phase constant increases exponentially, as the frequency increases. The attenuation constant increases when the lossy layer thickness increases up to $\Delta r = 1.5\delta$. The further increase in lossy layer thickness has negligible effect of attenuation constant [Figure 3.6(a)]. On the other hand, phase

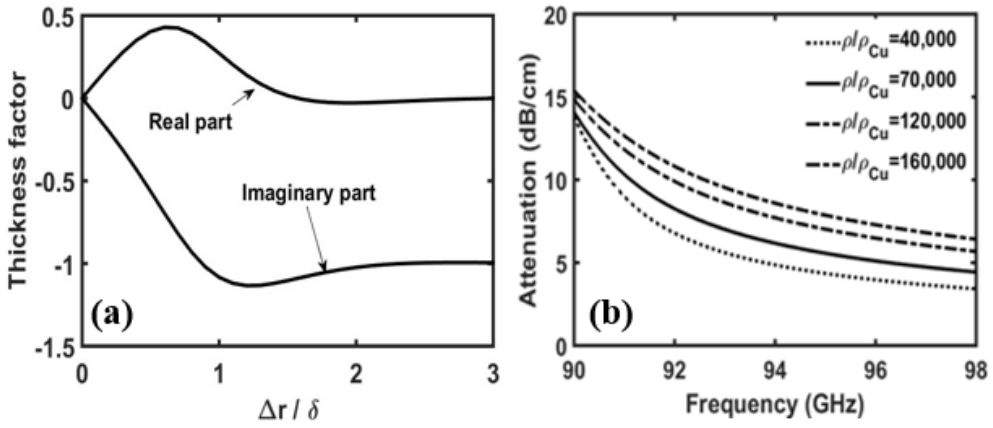


**Figure 3.5:** (a) Thickness factor Vs relative thickness of the lossy layer for $\rho/\rho_{Cu}$ =70,000, and (b) attenuation Vs frequency for different resistivity.

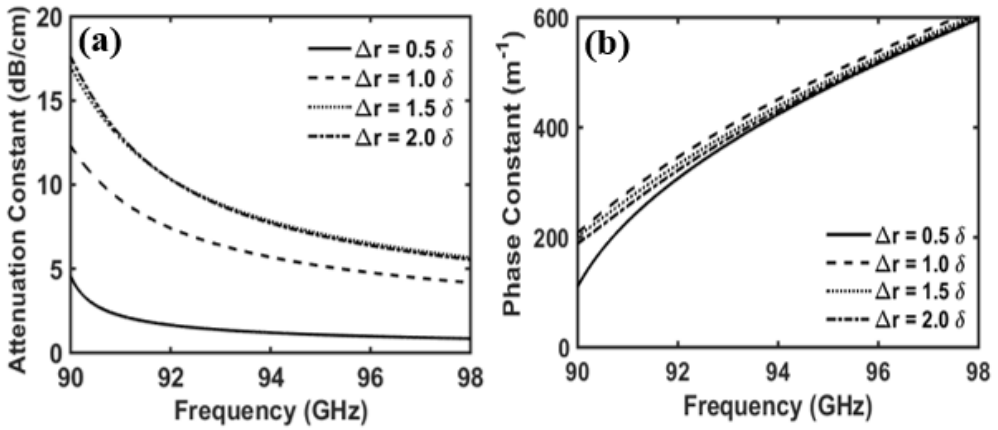


**Figure 3.6:** (a) Attenuation constant and (b) phase constant as a function of frequency for $TE_{01}$ mode ($\rho$ /$\rho_{Cu}$ =70,000).

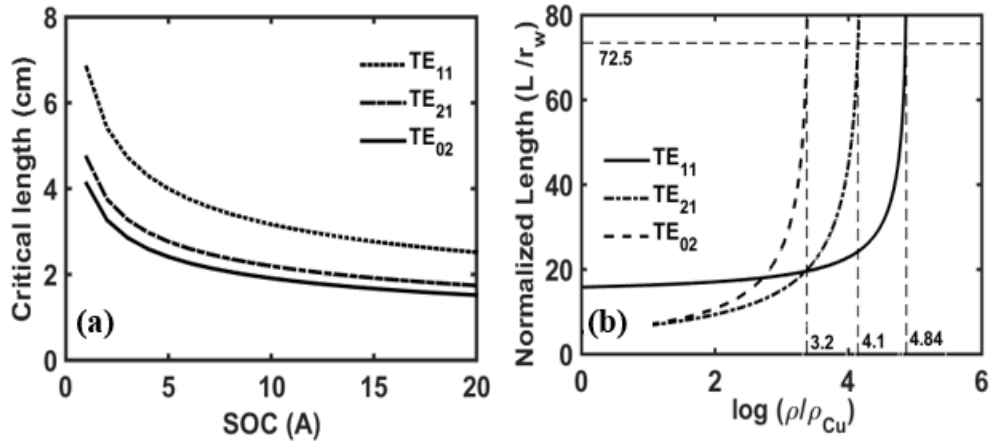


**Figure 3.7:** (a) Critical length Vs SOC of unloaded section and (b) start oscillation length of competing modes Vs resistivity.

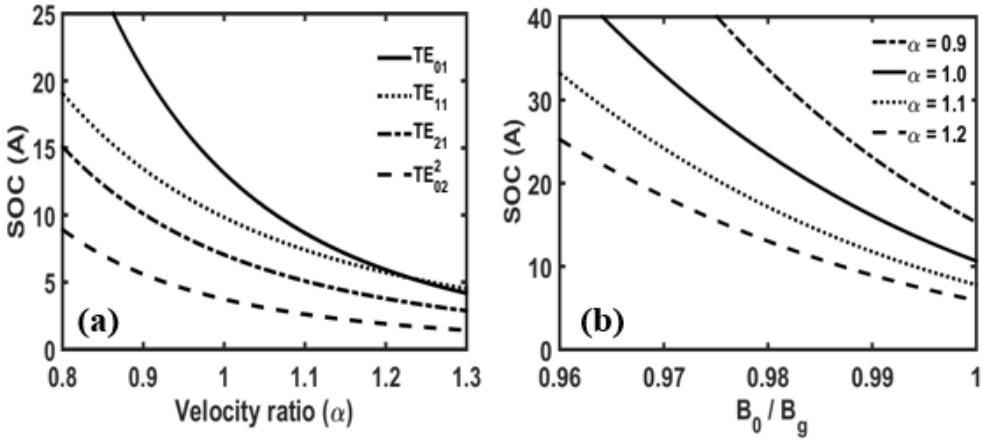


**Figure 3.8:** (a) SOC for operating and competing modes Vs velocity ratio (α) and (b) SOC of operating mode Vs grazing magnetic field for various α.

constant is nearly insensitive to the increase in lossy layer thickness[Figure 3.6(b)]. The stability of the present gyro-TWT is investigated by BWOs analysis of the interaction circuit [Tsai *et al.* (2004)]. The Figure 3.7(a) shows the relation between the critical length of the unloaded section and start oscillation current (SOC) for the competing backward wave oscillating modes including $TE_{11}$**,** $TE_{21}$, and $TE_{02}$ modes. It is observed that $TE_{02}$ mode is highly sensitive to the beam current and has lowest start oscillation length of 2.8 cm. Therefore, for the stable operation the length of the unloaded section is chosen to be 2.5 cm. The dependence of normalized circuit length ($L/r_w$) on resistivity of the lossy material for competing modes is shown in Figure 3.7(b). The $TE_{02}$ mode is found highly sensitive to resistivity and can be stabilized at low resistivity, while $TE_{11}$ mode is found to be least sensitive to the resistivity and required high attenuation for stabilization. The required resistivity for the stabilization of $TE_{11}$, $TE_{21}$ and $TE_{02}$ modes are $\log(\rho / \rho_{Cu}) = 4.84$, 4.1, and 3.2, respectively, with normalized circuit length ($L/r_w$) of ~72.5. SOC of the desired and spurious modes is monotonically decreased, as the velocity ratio ($\alpha$) increases [Figure 3.8(a)]. Similarly, SOC of operating $TE_{01}$ mode w.r.t normalized magnetic field $B_0 / B_g$ for the fixed values of α [Figure 3.8(b)] shows that it is decreased continuously.

### 3.4. PIC Simulation and Validation with Multimode Code

The design parameters of the present gyro-TWT are shown in Table 3.3. The RF interaction circuit is simulated in the absence of electron beam to calculate the required loss at operating frequency. A cylindrical waveguide of 12 cm length is uniformly coated with 0.05 mm thickness of resistive material and simulated for the propagation characteristics. The lossy section provides an insertion loss of ~90 dB to the operating $TE_{01}$ mode. Further, the beam present analysis is carried to calculate the amplified RF output, gain, and bandwidth of the present W-band gyro-TWT. The PIC simulation of the RF circuit along with an input coupler is done to study the multimode beam-wave interaction behavior. The input signal is fed through a rectangular port at the coupler end and an electron beam of 100 kV and 5 A with 5% spread is generated from the cylindrical cathode. The beam wave interaction occurs inside RF circuit, where the gyrating beam interacts with the cylindrical waveguide modes. The strength of the wave is weakened in the lossy section due to the attenuation and it gets maximum amplification in the unloaded section. The output electric field signal [Figure 3.9(a)] of the desired operating $TE_{01}$ mode and other spurious modes clearly shows that the field amplitudes of the spurious modes are very less as compared to the amplitude of operating mode. The frequency spectrum [Figure 3.9(b)] of the developed RF signal in $TE_{01}$ mode confirms the device operating frequency as ~92 GHz. The RF power developed in the desired operating $TE_{01}$ mode is ~140 kW, which is calculated by squaring the field amplitude (blue colored) shown in Figure 3.10(a), through post-processing technique in CST. Similarly, the power in all other competing modes including $TE_{11}$, $TE_{21}$, and $TE_{02}$ modes is calculated as ~450W, ~100W, and ~10W, respectively. The obtained simulation results are compared using multimode theory as discussed in Chapter 2. The growth of power along the axial length of RF interaction

circuit is calculated using a steady state multimode code. The lossy linear section provides heavy attenuation to the competing modes, including ~6.5 dB / cm to $TE_{11}$ mode (at ~67 GHz), ~11.30 dB /cm to $TE_{21}$ mode (77 GHz), and ~18.50 dB /cm to $TE_{02}$ mode (at 166.5 GHz), as compared to ~7.5 dB /cm to the operating $TE_{01}$ mode at 92 GHz. At these attenuation levels, SOC of the competing modes is over and above the operating current ~5 A. Therefore, all the competing modes are suppressed at their respective oscillation frequencies in the linear section. However, the operating $TE_{01}$ mode with its residual field from the linear section is excited in the non-linear section and grows exponentially, as shown in Figure 12. A maximum RF output power of ~145 kW is obtained in $TE_{01}$ mode, which is in close agreement with PIC simulated results (Figure 3.11). Further, negligible amount of powers in the competing modes, including ~1 W in $TE_{21}$, and ~100 W in both $TE_{11}$ and $TE_{02}$ modes, are observed through nonlinear multimode investigation (inset of Figure 3.11). The RF output power and bandwidth of the present gyro-TWT are observed by varying the resistivity of lossy material [Figure 3.12(a)]. Since, wall resistivity increases the threshold current limit of backward wave oscillation and the operating mode, hence the output power increases. There is a slight increase in the bandwidth of gyro-TWT, as the resistivity of lossy layer increases. The frequency response of the present gyro-TWT is observed for the range of 91-98 GHz and compared with experimental gyro-TWT results [Song *et al*. (2004)]. The 3-dB bandwidth of the amplifier is calculated as ~5 GHz for 5 % of axial velocity spread of the electron beam [Figure 3.12(b)]. The power gain of the present gyro-TWT obtained from the PIC and multimode simualtions are compared with the results of McDermott *et al.* [McDermott *et al.* (2002)] [Figure 3.13(a)]. Further, the transfer characteristic of gyro-TWT is benchmarked with an experimental gyro-TWT at 92.2 GHz [Song *et al*. (2004)] for the beam parameter of 70 kV and 5.3 A [Figure 3.13(b)].

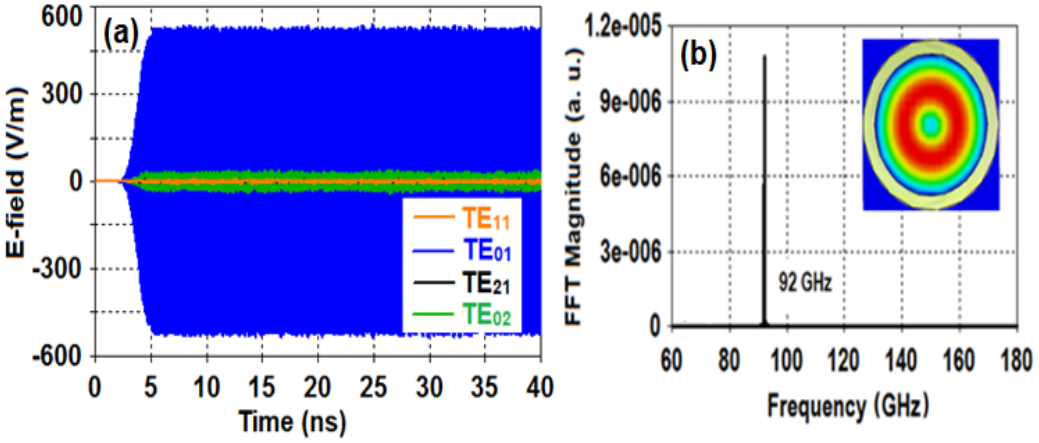


**Figure 3.9:** (a) Temporal response of the E-field of $TE_{01}$, $TE_{11}$, $TE_{21}$, and $TE_{02}$ mode using CST simulation (b) FFT magnitude and contour plot of the operating $TE_{01}$ mode at the output port.

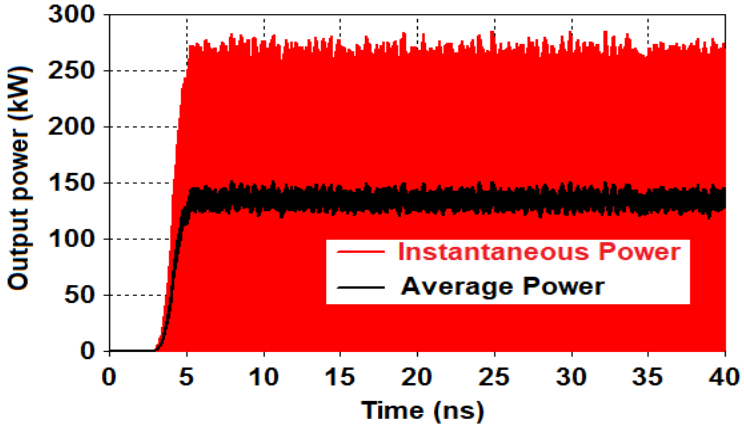


**Figure 3.10:** The RF output power growth rate of output power for operating.

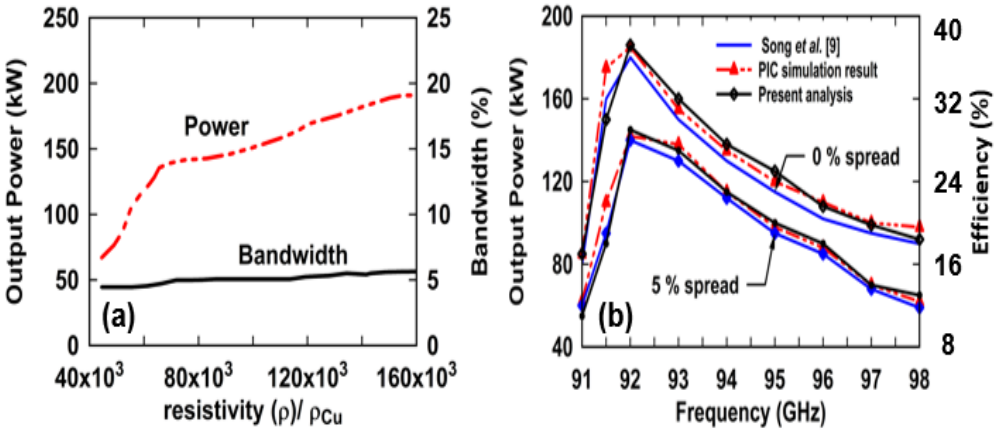


**Figure 3.11:** (a) Power and bandwidth Vs resistivity and (b) comparison of peak power and efficiency Vs Frequency ($V_0$ = 100 kV, $I_0$ = 5A).

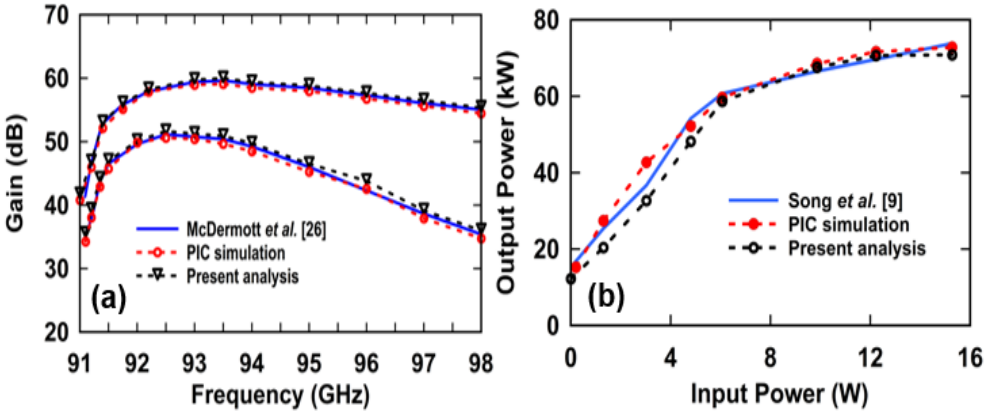


**Figure 3.12:** (a) Comparison of power gain Vs frequency ($V_0$ = 100 kV, $I_0$ = 5A) and (b) transfer characteristic of W-band UDL gyro-TWT ($V_0$ = 70 kV, $I_0$ = 5.3 A).

**Table 3.3:** Optimized Parameters List For W-Band Gyro-TWT.

| Parameters | Values |
|---|---|
| Operating Mode | $TE_{01}$ |
| Lossy wall resistivity | $70{,}000\rho_{Cu}$ |
| Beam Voltage (V) | 100 kV |
| Beam Current (I) | 5 A |
| Guiding Center radius ($r_g$) | 0.9648 mm |
| Larmor radius ($r_L$) | 0.22 mm |
| Velocity ratio (α) | 5 % |
| DC Magnetic Field, $B_0$ | 3.56 T |
| Total Lossy section length ($L_1$) | 12.0 cm |
| Copper circuit length ($L_2$) | 2.5 cm |

## 3.5. Design of the Output System of W-Band Gyro-TWT

### 3.5.1. Design of Undepressed Collector

The spent electrons are collected at the collector, which is also served as an output waveguide. The trajectory of the beam in collector region can be expressed as,

$$r = \sqrt{B_0 / B_c(z)}\left\{r_{g0} + r_{L0}\sin\phi(z)\right\} \tag{3.2}$$

where, $r_{g0}$ and $r_{L0}$ are the guiding center and Larmor radii in the interaction region, respectively, $B_0$ and $B_c(z)$ are the magnetic field strengths in the interaction circuit and at any point in the collector, respectively, and $\phi(z)$ is the phase of the electron. The magnetic field at the collector end is assumed ~ 0.016 T and the collector radius is

estimated as ~15 mm. For a peak RF power ($P_{RF}$) of 140kW and electron beam power ($P_e$) of 500 kW, the collector is designed to handle spent electron beam with an average beam power of 36 kW with 10 % duty cycle. Figure 3.14 shows the collector geometry and spent beam trajectory in the collector region using electron optics, *i.e.* E-GUN code. Considering the electron beam uniformly distributed over the length of 140 mm of the collector wall, the heat dissipating area is calculated as 131.95 $cm^2$ (2π x 1.5 cm x 14 cm). Hence, the maximum heat wall loading at the collector surface is 0.272 kW /$cm^2$. This is well below the technical limit of 1 kW /$cm^2$.

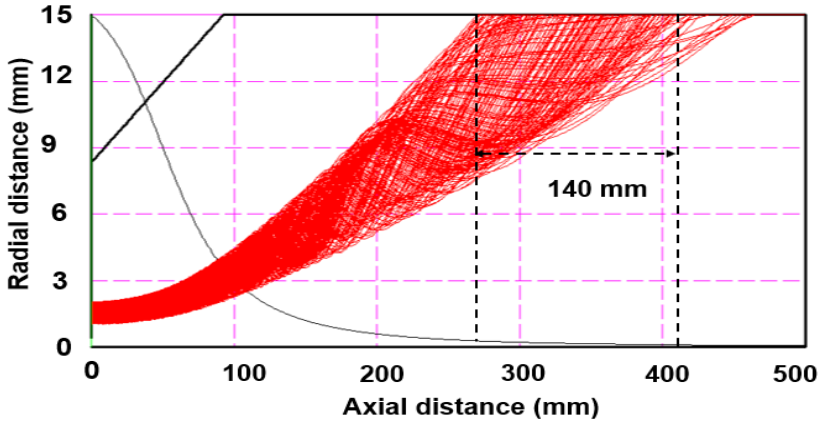


**Figure 3.13:** Beam trajectory in the 2D model of collector design using EGUN-code.

### 3.5.2. Design of Single Disc Output Window

To extract the RF output power, an output window is connected after the collector through a tapered waveguide. The microwave window is a passive device, which helps to isolate vacuum inside the device with outside atmosphere [Donaldson *et al.* (2013)]. In the present case, a single disc output window is designed and modeled [Figure 3.15(a)] using a ceramic material, alumina ($\varepsilon_r$ = 9.7), as it has high mechanical strength. The thickness of the disc is generally chosen to be $n\lambda_g/2$, where, $n$ is an integer, and $\lambda_g$ is the wavelength in the disc medium. The thickness and radius of RF window are calculated as 1.04 mm (n = 2) and 8 mm, respectively. The transmission and reflection coefficients [Figure 3.15(b)] are -0.05 dB and – 68dB at 92GHz, respectively.

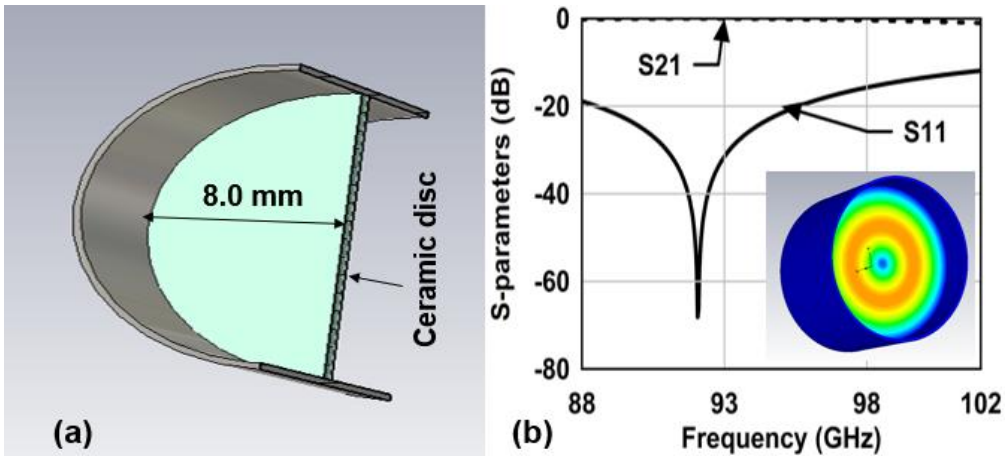


**Figure 3.14:** (a) CST model of RF output window for 92 GHz $TE_{01}$ mode Gyro-TWT and (b) S-parameter results of the output window.

## 3.6. Conclusion

A millimeter wave UDL gyro-TWT amplifier has been studied for its stability and beam-wave interaction behavior by revisiting the linear and multimode non-linear theories, respectively. The obtained multi-mode performances have been validated using a commercially available 3D PIC code. An output power of ~140 kW at 92 GHz with the saturated power gain of ~ 51 dB and 3-dB bandwidth of 5% has been achieved. The PIC simulation results are agreed by ~ 4% with the experimental W-band gyro-TWT [Song *et.al* (2004)]. The present dielectric loading has suppressed the spurious $TE_{11,}$ $TE_{21}$ and $TE_{02}$ modes and they have shared only negligible power as compared to the operating $TE_{01}$ mode. A single anode MIG has been designed and studied for the DC emission with 5% axial velocity spread and unity velocity ratio. A Y-shaped input coupler has been designed and studied for its propagation characteristics of 0.05 dB at 92 GHz. The present collector with the heat wall loading at its surface due to the spent beam was calculated as 0.255 kW/ $cm^2$. The output window has been found to be transparent to the operating $TE_{01}$ mode with low reflection over a wide bandwidth.